Crosslinkable High Dielectric Constant Polymer Dielectrics for Low Voltage Organic Field-Effect Transistor Memory Devices

Chih-Chien Hung,[1] Hung-Chin Wu,[2] Yu-Cheng Chiu,[2] Shih-Huang Tung,[1] Wen-Chang Chen[1,2]

[1]Institute of Polymer Science and Engineering, National Taiwan University, Taipei, 10617, Taiwan
[2]Department of Chemical Engineering, National Taiwan University, Taipei, 10617, Taiwan
Correspondence to: W.-C. Chen (E-mail: chenwc@ntu.edu.tw) or S.-H. Tung (E-mail: shtung@ntu.edu.tw)

Received 22 May 2016; accepted 10 June 2016; published online 1 July 2016
DOI: 10.1002/pola.28209

ABSTRACT: In this study, we successfully synthesized water/methanol soluble random copolymers with a high dielectric constant, poly(n-(hydroxymethyl) acrylamide-*co*-5-(9-(5-(diethylamino)pentyl)−2-(4-vinylphenyl)−9H-fluorene(P(NMA-*co*-F6NSt)), which contained chemical crosslinkable segment (NMA) and hole trapping building block (F6NSt). The feeding molar ratios of two monomers (NMA:F6NSt) were set as 100:0, 95:5, 80:20, and 67:33 for the copolymers of **P1**, **P2**, **P3,** and **P4**, respectively. The crosslinked P(NMA-*co*-F6NSt) thin film could serve as both dielectric and charge storage layers in organic field-effect transistor (OFET) memory device and exhibited high *k* (i.e., 4.91–6.47) characteristics, leading to a low voltage operation and a small power consumption. Devices based on the **P1**-**P4** dielectrics showed excellent insulating properties and good charge storage performance under a low operating voltage in a range of ±5V because of tightly network structures and well-dispersed trapping cites. In particular, **P3**-based memory device exhibited a large memory window of 4.13 V with stable data retention stability over 10^4 s, a large on/off ratio of 10^4, and good endurance characteristics as high as 200 cycles. The above results suggested that a high-performance OFET memory device could be facilely achieved using the novel crosslinkable high-*k* copolymers. © 2016 Wiley Periodicals, Inc. J. Polym. Sci., Part A: Polym. Chem. **2016**, *54*, 3224–3236

KEYWORDS: charge transport; crosslinking; dielectric properties; thin films

INTRODUCTION Organic field-effect transistor (OFET)-type memory devices have been widely investigated recently due to their advantages of nondestructive reading, low cost and easy-processability, as compared to the inorganic (e.g., metal oxide) counterparts.[1–10] Among numerous organic-based charge storage elements in the OFET memory community, nano-floating gate dielectrics and conjugated polymer-based electrets have been attracted extensive research interest owing to the efficient charge trapping.[11–25] The memory characteristics, such as charge storage capacity and data retention stability, are closely linked to the morphology of charge trapping sites and the strength of loaded electric field in the tunneling layer. Current reported OFET memory devices, however, normally possess relatively high operating voltages (> 30 V) and complicated processing procedures (insert an additional charge storage layer in a conventional OFET) to drive the device for digital data storage.[5,20,22–24] It would be of significant benefits to develop high dielectric constant (*k*) organic materials with both gate dielectric and charge storage functions for OFET memory devices.

Crosslinked poly(4-vinylphenol) (*c*-PVP) was commonly used as gate dielectric layer to obtain low-operating voltage OFETs (below 10 V) in the literatures because of its crosslinkable and high-*k* property.[26–29] The fabrication of high quality *c*-PVP blocking layer, however, is complicated, and needed to be processed under a nitrogen atmosphere since the oxygen and moisture in the air would destroy the crosslinking reaction between polymer and crosslinker. Leakage currents may easily appear in the devices based on *c*-PVP layer if the crosslinking reaction is insufficient.[26,29] The unreacted crosslinker aggregates in such *c*-PVP dielectric, in addition, would increase the surface roughness and lead to unstable device characteristics.[26,28,29] A self crosslinkable high-*k* polymer dielectric materials (i.e., without using an additional crosslinker), thus, is highly desired. Poly(n-hydroxymethyl acrylamide) (PNMA) is a well-known crosslinkable polymer, which possesses a self-condensable methylol group.[30] During the thermal crosslinking reaction, bis(methylene ether) group between NMA moieties would be firstly formed after dehydration, and then methylene bridge is generated by eliminating formaldehyde, as reported in the literatures.[30] This crosslinking reaction with the covalent bond formation is relatively stable compared to the ionic bond-assisted or physical crosslinking. Thus, crosslinked PNMA (*c*-PNMA) thin

Additional Supporting Information may be found in the online version of this article.

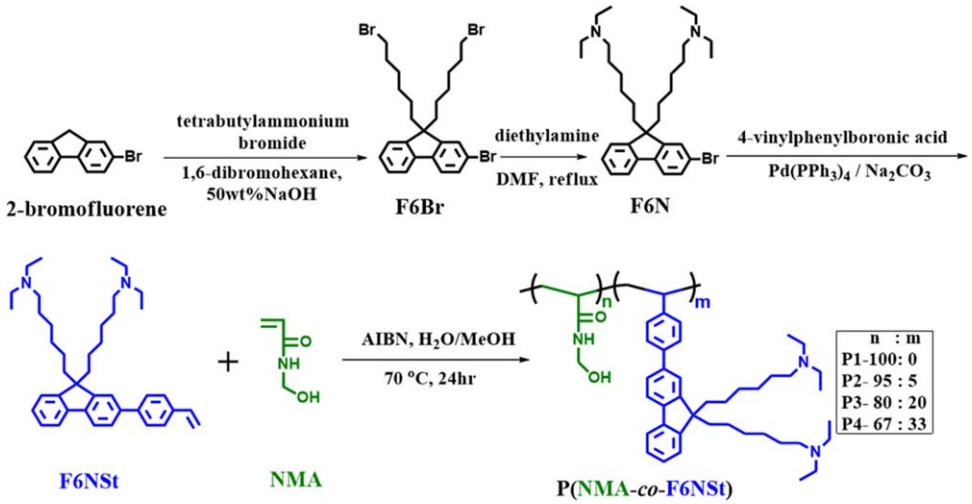

SCHEME 1 Synthetic route of F6NSt monomer and P(NMA-*co*-F6NSt) random copolymers. [Color figure can be viewed in the online issue, which is available at wileyonlinelibrary.com.]

film exhibits good physical, thermal, and electrical property because of its tightly networked structures, which can be served as dielectric layer in a OFET device without a current leakage. The *c*-PNMA thin film, more important, possesses the high-*k* nature that can effecintly reduce the power consumption of an OFET device. Note that low voltage operated OFET devices using *c*-PNMA as the gate dielectric layer, to the best of our knowledge, has not been reported yet.

Charge trapping element plays a crucial role in OFET memory devices for the digital information storage. Integration of effective high-*k* gate dielectrics with suitable charge trapping building blocks can form functional materials containing both charge blocking and storage characteristics for low voltage-driven OFET memories. Pendant conjugated moieties, such as fluorene,[11,13,21,22] thiophene,[11,14] or triphenylamine[31,32] had been reported as charge trapping materials previously and exhibited stable charge storage behavior with excellent retention stability.[11,13,14] Among them, the fluorene backbone can be efficiently functionalized with variant end groups on its the alkyl side chains. Hydroxyl and amino groups,[33,34] for example, providing the flexibility to design a charge trapping element that can be dissolved in low (e.g., chloroform, chlorobenzene) or high polarity (e.g., methanol, water) solvents.

Herein, we design and synthesize an amino-functionalized pendent fluorene (F6NSt) via side chain engineering that can compatible with NMA in high polarity solvent of methanol and water. Then, a new series of high-*k* random copolymers, poly(*n*-(hydroxymethyl)acrylamide-*co*-5-(9-(5-(diethylamino)pentyl)−2-(4-vinylphenyl)−9H-fluorene (P(NMA-*co*-F6NSt)s), containing chemical crosslinkable segment (NMA) and hole trapping building block (F6NSt) was developed (Scheme 1). The feeding molar ratios of two monomers (NMA:F6NSt) were set as 100:0, 95:5, 80:20, and 67:33 for the copolymers of **P1**, **P2**, **P3,** and **P4**, respectively. The crosslinked P(NMA-*co*-F6NSt) thin films could serve as both dielectric and charge storage layers in N,N'-bis(2-phenylethyl)perylene-3,4,9,10-bis(dicarboximide) (BEP-PTCDI)-based OFET memory device. They exhibited high-*k* characteristics, leading to an efficient charge trapping with a low voltage operation as well as a reduced power consumption. The studied devices based on P(NMA-*co*-F6NSt) dielectrics with a variant NMA/F6NSt ratio (**P1**-**P4**) achieved a large memory window up to 4.13 V with a operation voltage below ±5 V. Furthermore, stable data retention stability was exhibited over 10^4 s with a good endurance under 200 continuous operating cycles, suggesting their potential applications for high-performance OFET memory devices.

EXPERIMENTAL

Materials

N-hydroxyethyl acrylamide (NMA) and tetrakis(triphenylphosphine) palladium(0) was provided by Tokyo Chemical Industry, Japan. Azobisisobutyronitrile (AIBN) was purchased from Acros (Belgium) and re-crystallized from ethanol. 2-Bromo-9H-fluorene, tetrabutylammonium bromide, 1,6-dibromohexane, sodium hydroxide, and diethylamine were purchased from Aldrich Chemical and used without purification. *N*,*N*-Dimethylacetamide (DMAc) and *N*,*N*-dimethylformamide (DMF) were dried and distilled under N_2. The other solvents were commercially available and used as received. 2-bromo-9,9-bis(6-bromohexyl)−9H-fluorene (F6Br) and 6-(2-bromo-9 -(6-(diethylamino)hexyl)−9H-fluoren-9-yl)-*N*,*N*-diethylhexan-1-amine (F6N) were prepared according to the literature report (see Supporting Information for details).

Monomer Synthesis

6-(9-(6-(diethylamino)hexyl)−2-(4-vinylphenyl)−9H-fluoren-9-yl)-N,N-diethylhexan-1-amine (F6NSt). 2 g (3.6 mmol) of F6N, 4.2 g of sodium carbonate, 1.1 g (7.2 mmol) of 4-vinylphenylboronic acid and 83 mg (0.07 mmol) of tetrakis(-triphenylphosphine) palladium(0) were dissolved in 20 mL anhydrous DMAc. After three freeze-thaw cycles, the mixture was refluxed under vigorously stirring for 48 h. The reaction

TABLE 1 Compositions and Properties of Poly(NMA-*co*-F6NSt)s

Polymer	Composition[a] (NMA:F6NSt)	M_n[b] (g mol^{-1})	PDI[b]	T_d (°C)	T_g (°C)
P1	100:0	56,200	2.15	210.4	60.5
P2	95:5	52,610	2.20	226.3	70.3
P3	80:20	54,860	2.42	246.9	73.0
P4	67:33	50,440	2.52	263.3	80.4

[a] Molar ratio, estimated from ^{1}H-NMR.
[b] Determined by GPC using water as eluent.

was cooled down to the room temperature, and the mixture was passed through an Al_2O_3 column to remove the palladium catalyst. F6NSt (1.04 g, 49.9%) was obtained as a light yellow oil by chromatography with ethyl acetate/triethtyamine as the eluent. ^{1}H NMR (400 MHz, $CDCl_3$, δ (ppm)): 7.62–7.66 (2H), 7.54–7.56 (2H), 7.36–7.40 (2H), 7.26–7.31 (4H), 2.44–2.49 (q, 8H), 2.28–2.32 (t, 4H), 1.85–1.92 (t, 4H), 1.21–1.31 (m, 4H) 0.88–1.14 (m, 20H), 0.54–0.62 (m, 4H).

Synthesis of PNMA Homopolymer and P(NMA-co-F6NSt) Copolymers

PNMA and P(NMA-*co*-F6NSt) were synthesized by free radical polymerization using monomers of NMA and F6NSt, as shown in the Scheme 1. Poly(NMA-*co*-F6NSt) with different monomer ratio of 0, 5, 20, and 33% of F6NSt are denoted **P1, P2, P3,** and **P4**, respectively, as listed in Table 1. The concentration of AIBN used as the initiator was 0.002–0.003 M. The reaction mixture containing methanol/H_2O and monomers was degassed by bubbling argon for 30 min and then reacted at 70 °C for 24 h. In order to remove unreacted monomer, the mixture was diluted with methanol/H_2O and dialyzed against water with a Spectra/Por 6 dialysis membrane (molecular weight cutoff of 10,000 g mol^{-1}) for 72 h, with replacement of the water at every 12 h. The polymer was obtained after freeze-drying to remove solvent residue. Number-averaged molecular weight (M_n) and polydispersity index (PDI) of the studied polymers that estimated from gel permeation chromatography (GPC) are listed in Table 1. The details on the synthesis and characterization of **P1**-**P4** are described as the following:

Synthesis of P1.
A reaction mixture of 1.16 g (11.5 mmol) of NMA, 9.1 mg (0.003 mmol) of AIBN, and 20 mL mixed solvent (methanol/H_2O = 1/1 (v/v)) was used to afford a white solid (984 mg, yield: 84.6%). ^{1}H NMR (400 MHz, d-DMSO, δ (ppm)): 8.02–8.42 (1H, —N<u>H</u>CH$_2$OH), 5.48–5.12 (1H, NHCH$_2$O<u>H</u>), 4.46–4.64 (2H, —NHC<u>H$_2$</u>OH), 1.82–2.22 (1H, —CH$_2$C<u>H</u>—), 1.20–1.74 (2H, —C<u>H$_2$</u>CH—). Anal. Calcd. for $C_4H_7NO_2$ (%): C, 47.52; H, 6.98; N, 13.85; Found (%): C, 46.91; H, 7.07; N, 13.01.

Synthesis of P2.
A reaction mixture of 1.10 g (10.9 mmol) of NMA, 0.25 g (0.4 mmol) of F6NSt, 10.1 mg (0.003 mmol) of AIBN, and 20 mL mixed solvent (methanol/H_2O = 3/2 (v/v)) was used to afford a white solid (1.04 g, yield: 76.2%). ^{1}H NMR (400 MHz, d-DMSO, δ (ppm)): 8.04–8.42 (10H, —N<u>H</u>CH$_2$OH), 7.16–7.92 (6H, phenyl group and fluorene aromatic proton), 5.44–5.18 (10H, NHCH$_2$O<u>H</u>), 4.42–4.65 (20H, —NHC<u>H$_2$</u>OH), 1.78–2.22 (11H, —CH$_2$C<u>H</u>—, —CH$_2$C<u>H</u>—), 1.21–1.73 (21H, —C<u>H$_2$</u>CH—), 0.78–1.20 (2H, Ar— (CH$_2$C<u>H$_2$</u>(CH$_2$)$_4$NCH$_2$CH$_3$, Ar— (CH$_2$)$_3$C<u>H$_2$</u>(CH$_2$)$_2$NCH$_2$CH$_3$). Anal. Calcd. for $C_{118}H_{195}N_{21}O_{38}$ (%): C, 56.34; H, 7.81; N, 11.69; Found (%): C, 56.02; H, 7.37; N, 11.41.

Synthesis of P3.
A reaction mixture of 0.89 g (8.8 mmol) of NMA, 1.51 g (2.6 mmol) of F6NSt, 10.4 mg (0.002 mmol) of AIBN, and 24 mL mixed solvent (methanol/H_2O = 5/3 (v/v)) was used to afford a light yellow solid (1.64 g, yield: 68.2%). ^{1}H NMR (400 MHz, d-DMSO, δ (ppm)): 8.02–8.44 (10H, —N<u>H</u>CH$_2$OH), 7.16–7.92 (25H, phenyl group and fluorene aromatic proton), 5.42–5.22 (10H, NHCH$_2$O<u>H</u>), 4.40–4.66 (20H, —NHC<u>H$_2$</u>OH), 2.25–2.48 (10H, Ar— ((CH$_2$)$_5$C<u>H$_2$</u>NCH$_2$CH$_3$), 1.78–2.22 (13H, Ar— (C<u>H$_2$</u>(CH$_2$)$_5$NCH$_2$CH$_3$ —CH$_2$C<u>H</u>—, —CH$_2$C<u>H</u>—, 1.23–1.71 (23H, —C<u>H$_2$</u>CH—), 0.44–1.22 (10H, Ar— (CH$_2$(C<u>H$_2$</u>)$_4$CH$_2$NCH$_2$CH$_3$, Ar— ((CH$_2$)$_6$NCH$_2$C<u>H$_3$</u>). Anal. Calcd. for $C_{58}H_{90}N_6O_8$ (%): C, 69.71; H, 9.08; N, 8.41; Found (%): C, 69.29; H, 9.51; N, 7.99.

Synthesis of P4.
A reaction mixture of 0.75 g (7.4 mmol) of NMA, 2.3 g (3.9 mmol) of F6NSt, 9.9 mg (0.002 mmol) of AIBN, and 24 mL mixed solvent (methanol/H_2O = 2/1 (v/v)) was used to afford a light yellow solid (2.02 g, yield: 66.8%). ^{1}H NMR (400 MHz, d-DMSO, δ (ppm)): 8.08–8.41 (10H, —N<u>H</u>CH$_2$OH), 7.14–7.88 (41H, phenyl group and fluorene aromatic proton), 5.38–5.24 (10H, NHCH$_2$O<u>H</u>), 4.41–4.66 (20H, —NHC<u>H$_2$</u>OH), 2.25–2.41 (16H, Ar— ((CH$_2$)$_6$NC<u>H$_2$</u>CH$_3$), 1.78–2.22 (14H, Ar— (C<u>H$_2$</u>(CH$_2$)$_5$NCH$_2$CH$_3$ —CH$_2$C<u>H</u>—, —CH$_2$C<u>H</u>—), 1.23–1.71 (21H, —C<u>H$_2$</u>CH—), 0.46–1.24 (23H, Ar— (CH$_2$(C<u>H$_2$</u>)$_4$CH$_2$NCH$_2$CH$_3$, Ar— ((CH$_2$)$_6$NCH$_2$C<u>H$_3$</u>). Anal. Calcd. for $C_{50}H_{76}N_4O_4$ (%): C, 75.33; H, 9.61; N, 7.03; Found (%): C, 76.09; H, 9.15; N, 6.73

Fabrication of c-PNMA And c-P(NMA-co-F6NSt) Thin Films for OFET Memory Devices

PNMA and P(NMA-*co*-F6NSt) random copolymers (**P1~P4**) were firstly dissolved in deionized water with a concentrations of 30–60 mg mL^{-1}, and the solutions were filtered through 0.22 μm pore size of PTFE membrane syringe filters. The solution was spin-coated at 3000 rpm for 60 s on a highly doped Si wafer and thermally crosslinked at 110 °C for 24 h under vacuum as the dielectric layer. The thickness of the crosslinked dielectric layers were in a range of 60–180 nm based on different polymer solution concentration. Self-assembled monolayer (using *n*-octadecyl trichlorosilane (ODTS) as reactant) on crosslinked polymer surface, in addition, were treated by the reported procedures.[36] The semiconducting layer of BPE-PTCDI (~50 nm-thick) were thermally deposited on ODTS-modified and pristine *c*-PNMA or *c*-P(NMA-*co*-F6NSt) surface with a deposition rate of 0.4–0.5 Å s^{-1} at 90 °C under a vacuum level of approximately 3 $\times$ 10^{-7} Torr. Finally, the top-contact source and drain

electrodes were defined by 70 nm-thick gold through a regular shadow mask, and the channel length (L) and width (W) were 50 and 1000 μm, respectively.

Characterization

^{1}H NMR and spectra were obtained at room temperature on a Bruker DPX-400 (400 MHz for ^{1}H) spectrometer using d-DMSO and $CDCl_3$ as deuterated solvent. The molecular weight and molecular weight distribution of **P1-P4** were determined by gel permeation chromatography (GPC) was performed on a Lab Alliance RI2000 instrument (two column, MIXED-C and D from Polymer Laboratories) connected with one refractive index detector from Schambeck SFD Gmbh. All GPC analyses were performed on polymer/water solution at a flow rate of 1 mL min^{-1} and calibrated with polyethylene oxide. Fourier transform infrared (FTIR) spectra were recorded on a PerkinElmer spectrum 100 Model FTIR spectrometer with a resolution of 1 cm^{-1} and the number of scans being 4.

Thermal gravimetric analyses (TGA) were performed using a TA Q50 at a heating rate of 10 °C min^{-1} under a nitrogen flow (20 ml min^{-1}). Different scanning calorimetry (DSC) measurements were acquired using a TA Q100 calorimeter. An indium standard was used to calibrate the instrument and nitrogen was used as the purge gas. The UV-Vis absorption spectrum was recorded on a Hitachi U-4100 spectrophotometer. For the thin film spectra, the polymer was first dissolved in water (10 mg mL^{-1}), followed by filtering through a 0.45 μm pore size PTFE membrane syringe filter, and then spin-coated at a speed rate of 3000 rpm for 60 s onto a quartz substrate. Cyclic voltammetry (CV) was performed with the use of a three-electrode cell in which ITO was used as a working electrode. A platinum wire was used as an auxiliary electrode. All cell potentials were recorded with the use of an Ag/AgCl, KCl (sat.) reference electrode. The electrochemical properties of the polymer films were detected with 0.1 M anhydrous acetonitrile solution containing tetrabutylammonium perchlorate (TBAP) as the electrolyte.

The thickness of polymer film was measured with a Microfigure Measuring Instrument (Surfcorder ET3000, Kosaka Laboratory). Contact-angle measurements were made using CAM 110 (Creating Nano Tech). Atomic force microscopy (AFM) measurements were obtained with a NanoScope IIIa AFM at room temperature. Commercial silicon cantilevers with typical spring constants of 21–78 N m^{-1} was used to operate the AFM in tapping mode. The X-ray diffraction (XRD) data were collected at BL17A1 in National Synchrotron Radiation Research Center (NSRRC) of Taiwan using a Mar345 image plate detector with a sample-to-detector distance of 213 mm. The angle of incidence was set as 0.2°, and the experimental results were recorded in the range of q = 2–20 nm^{-1}.

All the measurements of the transistor memories were conducted using a Keithley 4200-SCS semiconductor parameter analyzer (Keithley Instruments Inc., Cleveland, OH), with a Remote PreAmp (4200-PA) in a N_2-filled glove box at room temperature. Triaxial cables were connected onto the probe station to minimize the background noise. The carrier mobility (μ) and threshold voltage (V_{th}) can be estimated from the slope and intercept of the linear plot of the square root of drain-to-source current $(I_{ds})^{1/2}$ versus the gate voltage (V_g) by the following equation within the saturation regime:

$$I_{ds} = \frac{WC\mu}{2L}\left(V_g - V_{th}\right)^2 \quad (1)$$

where C is the capacitance per unit area of dielectric layer and V_{th} is threshold voltage,

The gate capacitance per unit area is given by:

$$C = k\varepsilon 0/d \quad (2)$$

Where ε_o is the vacuum permittivity, k and d are the relative dielectric constant and thickness of the insulator layer. For capacitance measurements, metal-insulator-matal (MIM) structures were fabricated by depositing gold electrodes on the bare Si wafers. The capacitances (C) of the different gate dielectrics were measured at 5 kHz. The capacitance of the layer dielectrics was measured on MIM structures using a Keithley 4200-SCS instrument equipped with a digital capacitance meter (model 4210-CVU).

RESULTS AND DISCUSSION

Synthesis and Characterization of PNMA And P(NMA-*co*-F6NSt) Copolymers

Crosslinkable and methanol/water soluble random copolymers, P(NMA-*co*-F6NSt)s, were successfully designed and synthesized (Scheme 1). The hydroxyl group containing NMA segment can be easily dissolved in high polarity solvents and crosslinked using thermal treatment. The conjugated fluorene moiety, however, usually can be only dissolved in a low polarity solvent, such as chloroform and dichloromethane. To improve the solubility of fluorene motif in methanol or water, its alkyl side chain was functionalized with amine end group, as depicted in Scheme 1. The ^{1}H NMR characteristics of fluorene-based monomers (i.e., F6Br, F6N, and F6NSt) are summarized in Supporting Information Figure S1.

Four P(NMA-*co*-F6NSt)s (**P1**∼**P4**) were obtained with different NMA/F6NSt ratios using a free radical copolymerization under a methanol/H_2O mixing solvent. The feeding molar ratios of two monomers (NMA:F6NSt) were set as 100:0, 95:5, 80:20, and 67:33 for **P1**, **P2**, **P3** and **P4**, respectively, and detailed polymer characteristics are listed in Table 1. The chemical structures and NMA/F6NSt compositions of the studied polymers were confirmed by ^{1}H NMR (Fig. 1) and elemental analysis. The signals c, e and d (8.08–8.41 ppm (-N$\underline{H}$CH$_2$OH), 5.38–5.24 ppm (—NHCH$_2$O$\underline{H}$) and 4.45–4.62 ppm (—NHC$\underline{H}_2$OH)) are attributed to the protons on NMA moiety, respectively; while the peaks of g (7.16–7.92 ppm (aromatic protons)), i (2.25–2.41 ppm (Ar—(CH$_2$)$_6$NC$\underline{H}_2$CH$_3$)) and h (0.46–1.24 ppm, (Ar—CH$_2$(C$\underline{H}_2$)$_4$ CH$_2$NCH$_2$C$\underline{H}_3$ and Ar— (CH$_2$)$_6$NCH$_2$C$\underline{H}_3$)) are the protons on F6NSt segment. The numbers of aliphatic or aromatic protons are estimated from the integration value of the signals, which are

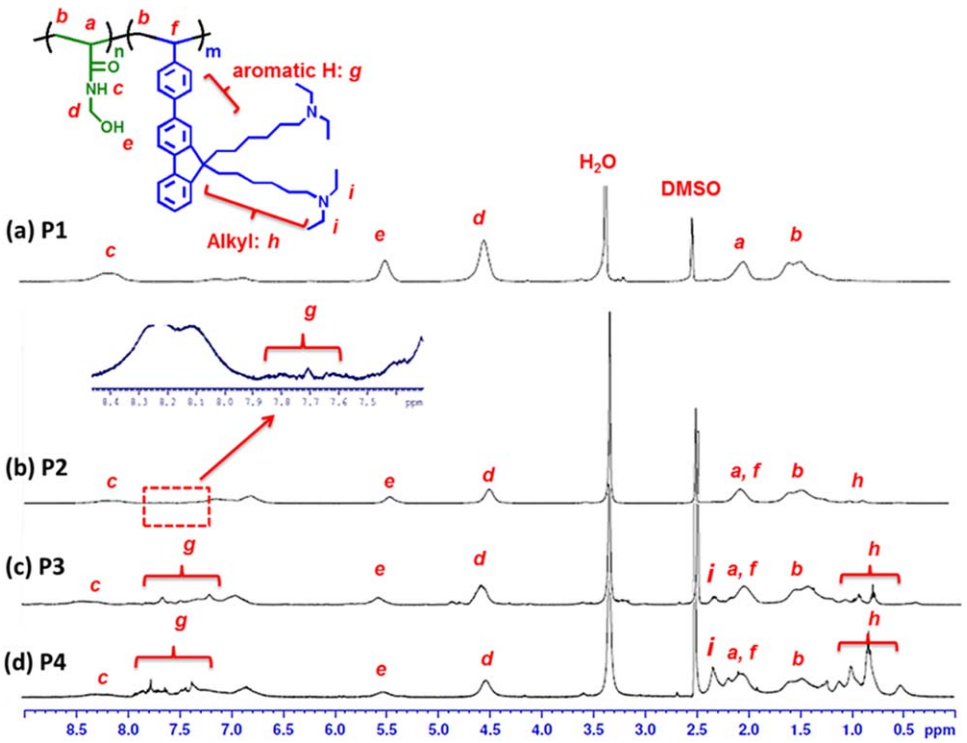

FIGURE 1 ^{1}H NMR spectra of (a) **P1**, (b) **P2**, (c) **P3**, and (d) **P4**, respectively, in d-DMSO. [Color figure can be viewed in the online issue, which is available at wileyonlinelibrary.com.]

consistent with the proposed polymer structures with different NMA/F6NSt ratio. The elemental analyses of the carbon, hydrogen, and nitrogen contents, additionally, illustrate a good agreement with the theoretical content. The number-averaged molecular weight (M_n) of **P1**, **P2**, **P3,** and **P4** are determined as 56,200, 52,610, 54,860, and 50,440 g mol^{-1} with a polydispersity index (PDI) value of 2.15, 2.20, 2.42, and 2.52, respectively, from GPC measurement (Table 1). Note that all the studied polymers are soluble in water and methanol, providing the solution-processable thin films for electronic device applications.

Thermal Properties

The thermal behaviors, including thermal decomposition temperatures (T_d, 5% weight loss) and glass transition temperatures (T_g), of the studied polymers were evaluated by thermogravimetric analysis (TGA) and differential scanning calorimetry (DSC) under a nitrogen atmosphere, respectively, as shown in Supporting Information Figure S2. The T_d of **P1**, **P2**, **P3,** and **P4** are 210, 226, 247, and 263 °C, respectively. It is clearly observed that the T_d becomes higher with the composition of stiff fluorene moiety. On the other hand, the T_g obtained from DSC curves are 61, 70, 73, and 80 °C of **P1**, **P2**, **P,3** and **P4**, respectively. The T_g of the set of polymers is raised as the content of fluorene segment increased, which is consistence with our previous study of pendent fluorene-based polymers.[13,36]

Optical and Electrochemical Properties

The UV-vis absorption spectra of fluorene monomer (F6NSt), **P2**, **P3**, and **P4** in thin film state are shown in Figure 2(a). The absorption maximum wavelengths (λ_{max}) of F6NSt is located at 312 nm; while λ_{max} of those P(NMA-*co*-F6NSt)s (**P2**∼**P4**) are slightly blue shifted to ∼308 nm due to the incorporation of non-conjugated NMA segment. The corresponding optical band gaps (E_g^{opt}) of F6NSt, **P2**, **P3**, and **P4** estimated from the onset of the solid state absorption using an empirical equation ($E_g^{opt} = 1240/\lambda_{onset}$), in addition, are calculated to be 3.50, 3.55, 3.56, and 3.56 eV, respectively.

On the other hand, the energy levels of the studied polymers are investigated using electrochemistry method. The cyclic voltammetry (CV) curves of F6NSt, **P2**, **P3**, and **P4** thin films are shown in Figure 2(b). The highest occupied molecular orbital (HOMO) levels were estimated from onset oxidation potentials (E_{onset}^{ox}), which based on the equations: HOMO-$= -e[E_{onset}^{ox} - E_{1/2}^{ferrocene} + 4.8]V$; while the lowest unoccupied molecular orbital (LUMO) levels were determined on the difference between HOMO and E_g^{opt} value (i.e., LUMO = HOMO − E_g^{opt}). From the CV traces, the E_{onset}^{ox} are 1.40, 1.44, 1.46, and 1.46 V versus Ag/Ag$^+$ reference electrode for F6NSt, **P2**, **P3**, and **P4**, respectively, and their corresponding HOMO energy levels are calculated to be −5.72, −5.76, −5.78, and −5.78 eV, respectively. Indeed, the LUMO levels are defined of approximately −2.20 eV, respectively.

Crosslinkable Polymer Dielectrics

The main reason of designing NMA segment in the studied polymers is not only to improve the solubility in water or methanol, but also to induce the crosslinking reaction of such polymer thin film under heat, leading to good dielectric

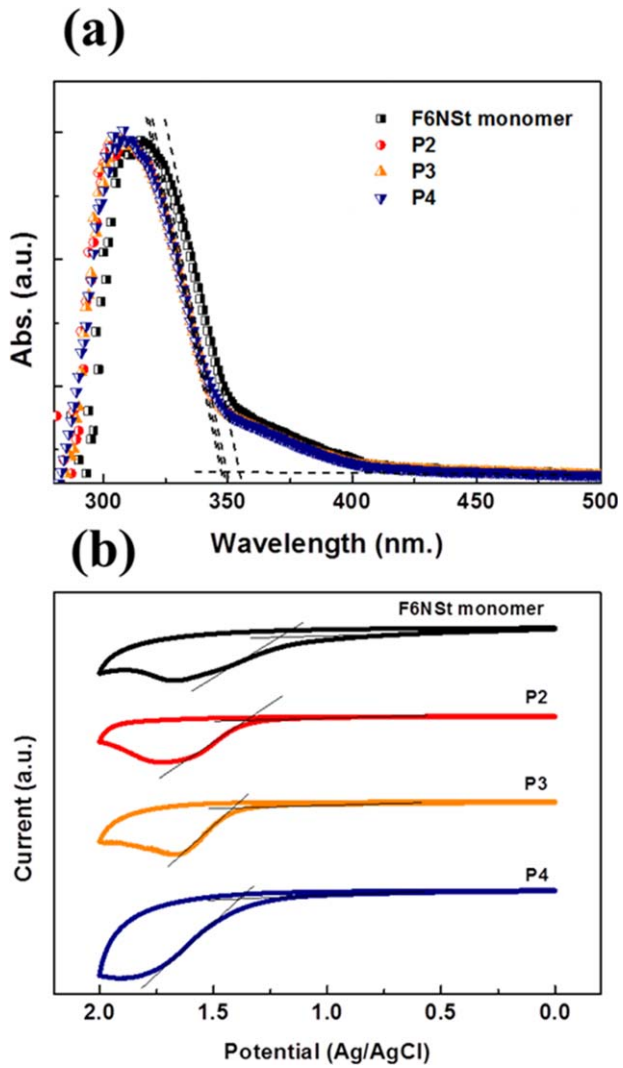

FIGURE 2 (a) UV-vis absorption spectra of the F6NSt and P(NMA-*co*-F6NSt) (**P2**∼**P4**) thin films. (b) Cyclic voltammograms of F6NSt and P(NMA-*co*-F6NSt) (**P2**∼**P4**) measured in 0.1 M TBAP/acetonitrile solution. [Color figure can be viewed in the online issue, which is available at wileyonlinelibrary.com.]

properties with low leakage current in the OFET application. An interesting characteristic can be clearly observed that the PNMA (**P1**) solution became more and more gelatinous and formed a hydrogel state after thermal crosslinking for 24 h (Supporting Information Fig. S3). The strong intermolecular binding via crosslinking between polymer chains significant increase the viscosity of the PNMA solution. The P(NMA-*co*-F6NSt) solution (e.g., **P2**), similarly, exhibits that the significant transition from solution state to hydrogel state via thermal curing. Moreover, the P(NMA-*co*-F6NSt) solution can emit blue color under UV light owing to the F6NSt moiety.

The crosslinking behaviors of the studied polymers were also investigated in thin film state. The polymer thin films were spin-coated using the solutions without thermal treatment, then the pristine films were crosslinked at 120 °C for 24 h under vacuum. Fourier transform infrared spectroscopy (FTIR) was used to demonstrate the studied polymer films are crosslinked successfully or not, as exhibited in Figure 3. For both uncured **P1** and **P2**-based films possess a broad peak at 3100–3500 cm^{-1}, which belongs to the O—H (3300–3500 cm^{-1}) and N—H (3100–3300 cm^{-1}) stretching of hydroxyl (—OH) and amide (—CONH) functional groups on NMA segment, respectively. After thermal crosslinking, the peak of hydroxyl group is significantly diminished in the crosslinked polymer thin films (*c*-PNMA and *c*-P(NMA-*co*-F6NSt)), and the signal is shifted to 3100–3300 cm^{-1}, containing only N—H stretching of amide group. The results demonstrate that the studied polymers can be effectively crosslinked through the dehydration of hydroxyl group on NMA segment. This crosslinking reaction, more importantly, can be proceeded without adding extra cross-inkers, providing a facile pathway to fabricate smooth and uniform dielectric thin film in OFETs. Note that **P3** and **P4** also exhibit similar FTIR results with crosslinkable thin film characteristics, as shown in Supporting Information Figure S4.

The surface structure of the crosslinked polymer thin films was recorded using atomic force microscopy (AFM), as shown in Supporting Information Figure S5. The *c*-PNMA (*c*-**P1**) and *c*-PNMA-*co*-F6NSt (*c*-**P2**-**P4**) films exhibit a smooth surface with a roughness of 0.169, 0.231, 0.522, and 1.812 nm, respectively. A relatively large roughness was explored on *c*-**P4** surface compared to other polymers because of the higher F6NSt content, which leads to the aggregations of fluorene moiety. Such crosslinked thin film, moreover, was immersed into toluene and chloroform for more than 2 h to make sure the polymer dielectric would not be destroyed by common organic solvents [using *c*-**P1** as example; Supporting Information Fig. S5(e,f)]. Uniform surface with a roughness of approximately 0.2–0.3 nm can be still maintained for the treated surface, indicating the studied crosslinked thin films possess strong covalent crosslinking

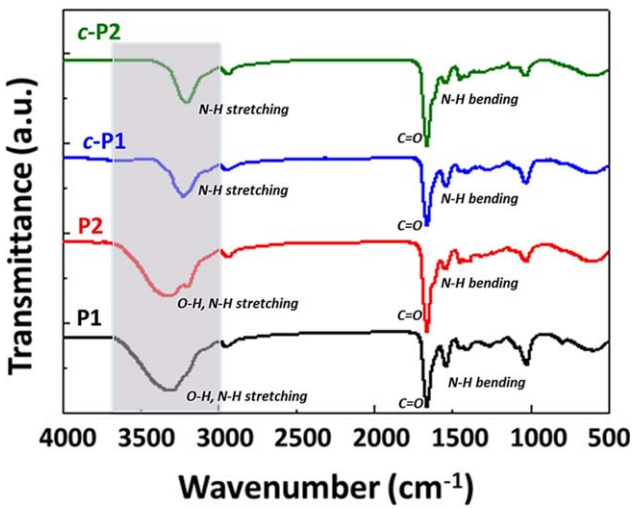

FIGURE 3 FTIR spectra of **P1** and **P2** films before and after the crosslinking reaction. [Color figure can be viewed in the online issue, which is available at wileyonlinelibrary.com.]

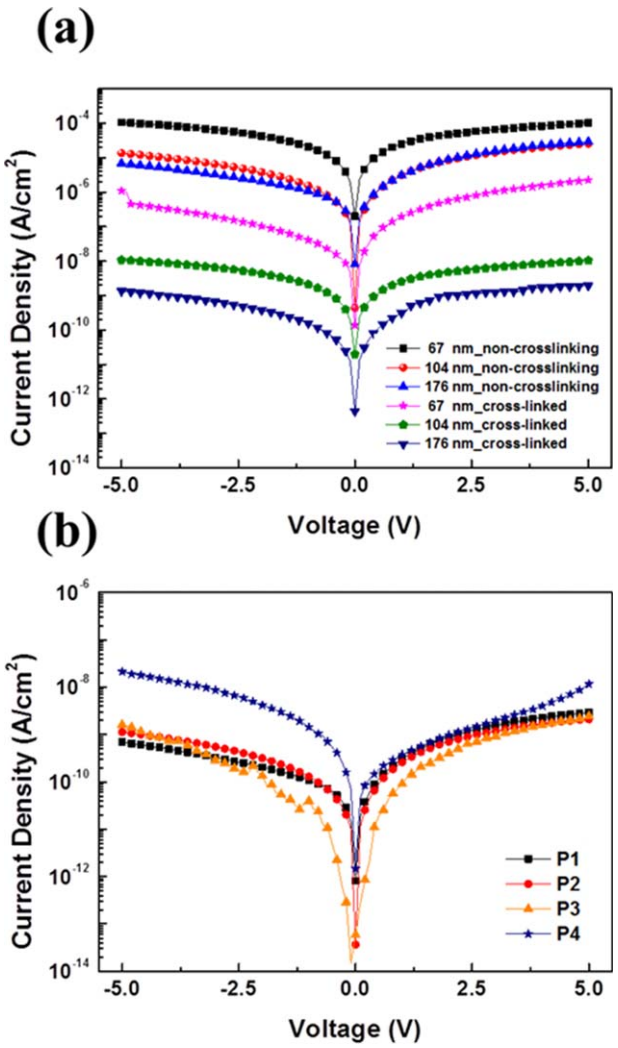

FIGURE 4 (a) The current density of non-crosslinked and crosslinked PNMA gate dielectrics thin film with different thickness. (b) The current density of **P1**, **P2**, **P3,** and **P4** dielectrics with a 160–180 nm-thick film. [Color figure can be viewed in the online issue, which is available at wileyonlinelibrary.com.]

structure and show excellent organic solvents resistance. Also, it provides a great potential to modify the hydrophobicity of the dielectric surface using solution process and further enhance the device performance.

Dielectric Properties

The quantitative dielectric constants, capacitances, and leakage currents of the gate dielectrics based on the studied *c*-PNMA and *c*-P(NMA-*co*-F6NSt) thin films were investigated (Fig. 4). The dielectric thin film was squeezed between top and bottom electrodes to integrate a metal/insulator/metal (MIM) device configuration. The measured leakage currents of PNMA (**P1**) dielectrics with variant film thickness in a range of 60–180 nm are explored in Figure 4(a). The non-crosslinked thin films exhibit high current levels at 10^{-4}–10^{-5} A cm^{-2}; while the currents are significantly reduced to 10^{-6}–10^{-9} A cm^{-2} for those thin films after crosslinking (i.e., *c*-**P1**), which is comparable with that of crosslinked PVP films with similar film thickness (10^{-6}–10^{-8} A cm^{-2}).[26,29,35] Note that for both non-crosslinked and crosslinked dielectrics, the current density is level downed with the increase of film thickness. The result demonstrates that the studied *c*-PNMA film can prevent the leakage current from passing through the dielectric layer in vertical direction effectively due to its tightly structural networks. Not only *c*-PNMA but also *c*-P(NMA-*co*-F6NSt) (**P2**, **P3,** and **P4**) thin films show low leakage currents (i.e., 10^{-8}–10^{-9} A cm^{-2}) as the film thickness is controlled at 160–180 nm [Fig. 4(b)]. The *c*-**P4** thin film, however, exhibits slightly higher current leakages due to the lower crosslinking density NMA domain (NMA/F6NSt: 67/33%) in the film compared to those of *c*-**P1**, **P2,** and **P3** films.

The dielectric constants and capacitances of the *c*-PNMA and *c*-P(NMA-*co*-F6NSt)s, furthermore, are probed and summarized in Supporting Information Table S1. Among the studied polymers, **P1** possesses a relatively high dielectric constant of 6.47 along with a capacitance of 34.08 nF cm^{-2} with 170 nm-thick film, which is several times higher than that of common dielectric polymers.[26,27,35] Note that the dielectric constant is reduced from 6.47 (**P1**) to 4.91 (**P4**) owing to the content of NMA in the studied copolymers is decreased. However, the dielectric constants of the studied polymers are still high enough to drive the OFET device under a low voltage, which can efficiently reduce the power consumption for high performance organic electronic applications.

Low-Voltage OFET Device

The OFETs using high-*k* *c*-PNMA as gate dielectric were fabricated with a BEP-PTCDI based device structure and their typical and transfer and output characteristics are depicted (Fig. 5). The BEP-PTCDI/*c*-PNMA-based device possesses an electron mobility of 8.22×10^{-4} cm^{2}V^{-1}s^{-1} with an on/off ratio of approximately 10^3 under an operating voltage below 5 V. The OFET performance can be further improved through the surface modification on the *c*-PNMA dielectric layer. Self-assembled monolayer of ODTS was then treated, and the mobility was largely enhanced to 1.34×10^{-2} cm^{2}V^{-1}s^{-1} with an on/off ratio of 10^4. Such significant improvement of OFET characteristics are mainly attributed to the changes of surface hydrophobicity on the *c*-PNMA dielectric as well as the crystallinity of BEP-PTCDI active layer.[37,38] Higher order X-ray diffraction peaks and larger grain size (522.5 ± 34.1 nm) can be explored of BEP-PTCDI thin film on ODTS-modified *c*-PNMA layer using AFM and grazing-incidence X-ray diffraction (GIXD) technique, as shown in Figure 6 and Supporting Information Figure S7. The above results demonstrate that the newly designed high-*k* *c*-PNMA dielectric can induce stable OFET characteristics using a small operating voltage with low leakage currents.

Next, BEP-PTCDI-based OFET using *c*-P(NMA-*co*-F6NSt) dielectrics were also investigated. Output and Transfer characteristics of such devices are depicted in Figure 5(c,d) and Supporting Information Fig. S6, and their electrical

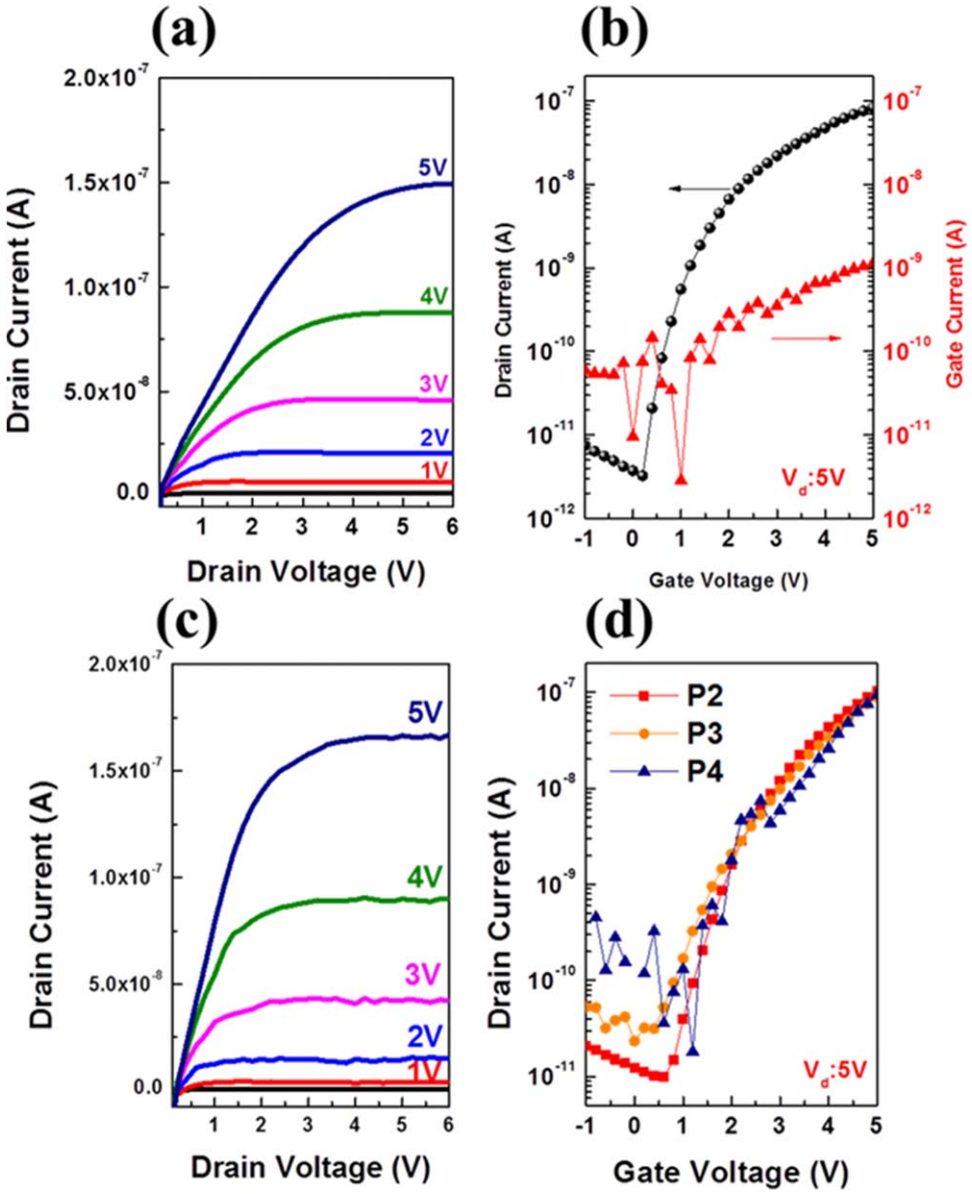

FIGURE 5 BEP-PTCDI-based OFET output curves using the dielectric layers of (a) **P1** and (c) **P3**; transfer characteristics using the dielectric layers of (b) **P1** and (d) **P2**∼**P4**. All dielectrics were modified with ODTS self-assembly monolayer. [Color figure can be viewed in the online issue, which is available at wileyonlinelibrary.com.]

properties are summarized in Table 2. The electron mobility of *c*-**P2**, **P3**, and **P4** dielectric-based transistors are 8.98×10^{-4}, 9.66×10^{-4}, and 6.90×10^{-4} $cm^2V^{-1}s^{-1}$ with an on/off ratio of 10^2-10^3 without a surface modification on dielectric layer. Note that lower charge carrier mobility is obtained in **P4**-based device than others, which is owing to the lower content of crosslinkable NMA domain in **P4**, resulting in a higher leakage current [see Fig. 4(b)]. Similarly to *c*-PNMA (**P1**), the mobility of *c*-P(NMA-*co*-F6NSt) (**P2**-**P4**)-based devices can be enhanced up to 1.59×10^{-2} $cm^2V^{-1}s^{-1}$ with high on/off ratio of 10^4 after the ODTS treatment. The enhancement of the electrical properties is also attributed to the hydrophobic dielectric surface after the ODTS modification, which can induce higher crystallinity of BEP-PTCDI thin film. Contact angle analysis (Supporting Information Fig. S8) demonstrates the studied ODTS-modified hydrophobic dielectric surfaces possess a high contact angle of 105°–110° compared to that of without the surface treatment (ca. 54°–76°). The nanorod-like BPE-PTCDI crystals, indeed, are induced on the ODTS-treated surfaces with larger grain sizes, as shown in Supporting Information Figure S9, resulting in better OFET performance for OFET memory device applications.

OFET Memory Device

Since low voltage operated OFET device can be achieved using the studied dielectric copolymers, as discussed in the previous section. The *c*-P(NMA-*co*-F6NSt) thin films (i.e., **P2**,

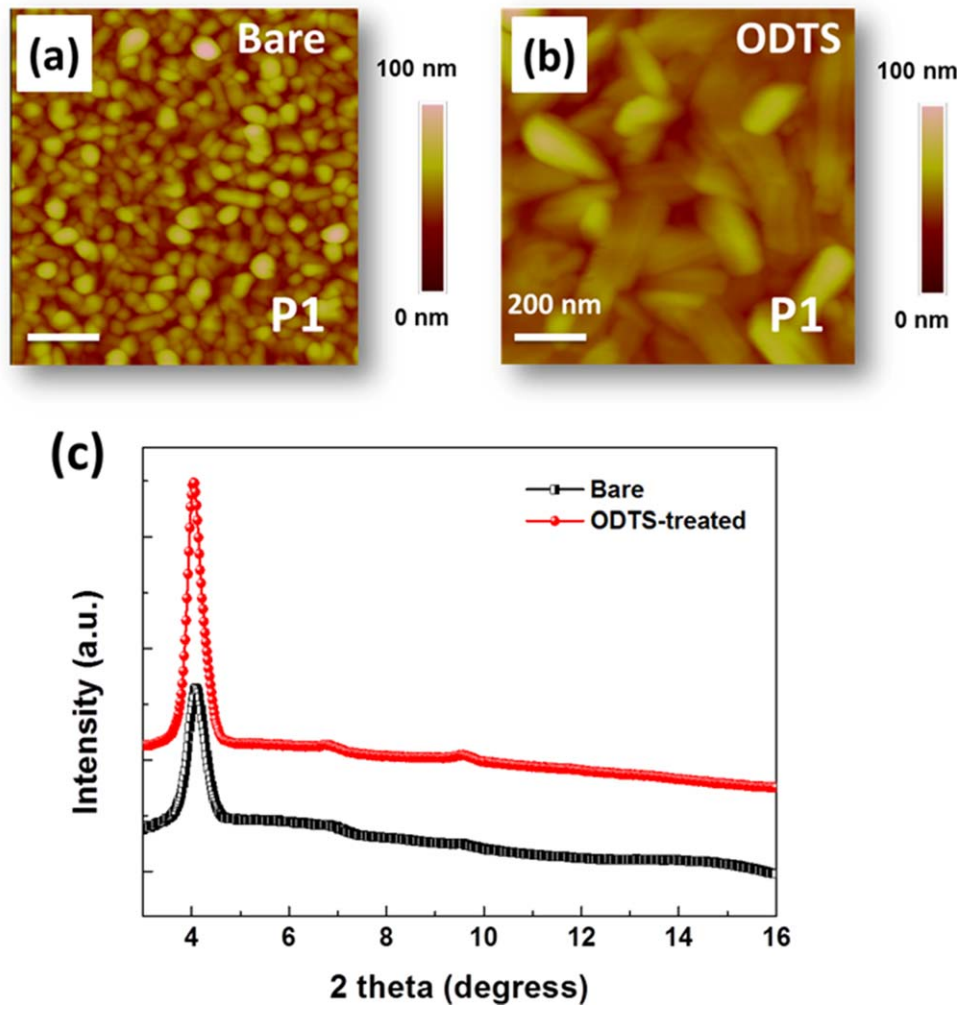

FIGURE 6 AFM topographies of the BPE-PTCDI thin film deposited on (a) bare and (b) ODTS-treated *c*-**P1** dielectric. (c) 1D X-ray diffraction profile of the BPE-PTCDI thin film on bare and ODTS-treated *c*-**P1** dielectric. [Color figure can be viewed in the online issue, which is available at wileyonlinelibrary.com.]

P3, and **P4**) are further used as both gate dielectric and charge storage layer in BPE-PTCDI-based OFET memory devices [Fig. 7(a)], owing to the well-dispersed F6NSt moiety can be served as charge trapping site. The memory characteristics and summarized parameters are in Figure 7(b,c) and Supporting Information Figs. S10–S12 and Table 2, respectively. To switch the conductance of memory devices, an external pulse of the gate voltage is applied to adjust

TABLE 2 Characteristics of BPE-PTCDI-based OFET Memory Devices using *c*-P(NMA-*co*-F6NSt) Dielectrics

Polymer	Surface Modification	Mobility ($cm^2V^{-1}s^{-1}$)	On/off Ratio (−)	Memory Window (V)
P1 (PNMA)	Bare	$(8.22 \pm 0.05) \times 10^{-4}$	1.4×10^3	–
P1 (PNMA)	ODTS	$(1.34 \pm 0.13) \times 10^{-2}$	3.6×10^4	–
P2 (95:5)[a]	Bare	$(8.98 \pm 0.31) \times 10^{-4}$	1.2×10^3	1.28 ± 0.65
P2 (95:5)[a]	ODTS	$(1.37 \pm 0.08) \times 10^{-2}$	1.7×10^4	1.31 ± 0.14
P3 (80:20)[a]	Bare	$(9.66 \pm 0.11) \times 10^{-4}$	1.4×10^3	3.90 ± 0.52
P3 (80:20)[a]	ODTS	$(1.59 \pm 0.09) \times 10^{-2}$	1.2×10^4	4.13 ± 0.32
P4 (67:33)[a]	Bare	$(6.90 \pm 0.55) \times 10^{-4}$	2.2×10^2	4.61 ± 0.38
P4 (67:33)[a]	ODTS	$(1.35 \pm 0.09) \times 10^{-2}$	1.0×10^4	4.83 ± 0.11

[a] The ratio in the parentheses is the mole ratio of NMA to F6NSt.

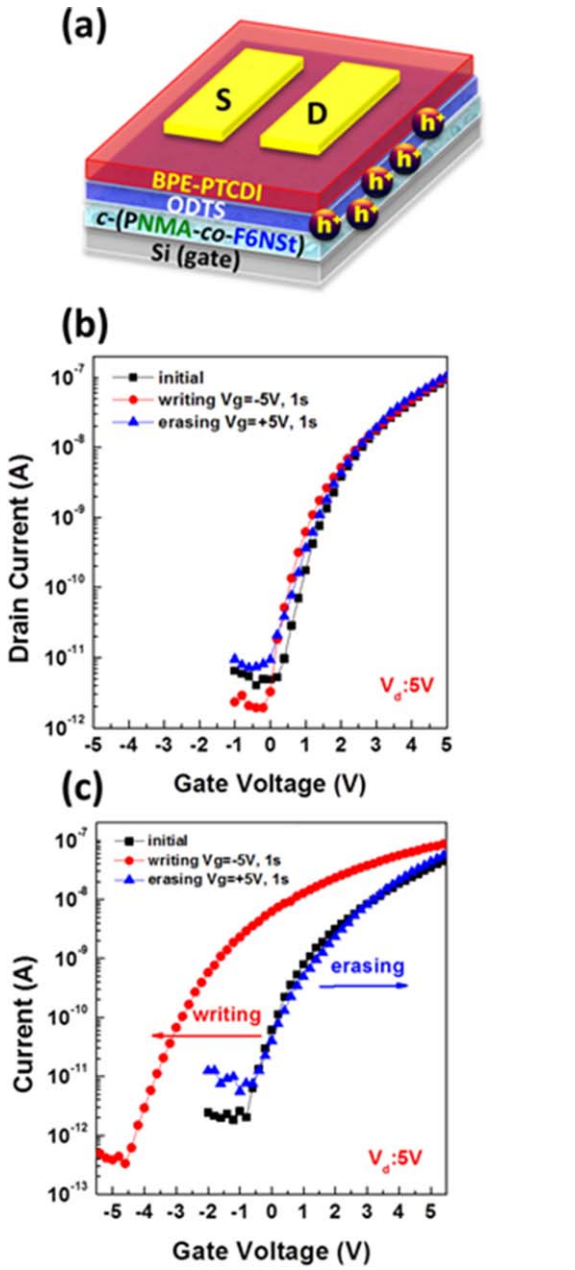

FIGURE 7 (a) Schematic structure of the *c*-P(NMA-*co*-F6NSt) dielectric-based OFET memory device. Transfer characteristics of BEP-PTCDI-based OFET memory devices using gate dielectric and charge trapping layers of (b) **P1** and (c) **P3**, respectively. [Color figure can be viewed in the online issue, which is available at wileyonlinelibrary.com.]

the electric field and storage the charges into the dielectric layer. The BPE-PTCDI-based devices, thus, were operated by applying an appropriate gate pulse (±5 V) for 1 s to control the charge storage and release state (i.e., ON and OFF state) of the memory devices. When a negative gate bias ($V_g = -5$ V, 1 s) is applied, a negative shift is observed on the transfer curve, which is cause by the induced hole injection from the semiconductor layer into the dielectric layer. This phenomena, moreover, is defined as the writing process. On the contrary, a positive gate bias ($V_g = 5$ V, 1 s) would generate the electron injection into the dielectric and lead to a positive shifting of transfer curve, referred to as the erasing process. It is worth to noting that the capacity of digital information storage, called memory window, is defined as the threshold voltage difference between writing and erasing state. The calculated memory window of the OFET memories using *c*-**P2**, **P3**, and **P4** dielectric and charge storage layer is 1.28, 4.13, and 4.83 V, respectively. The memory capacity is significantly enlarged as the content of the fluorene moiety increased. It is worth to mention that a highest charge storage density (~0.48) of the studied copolymers, which is calculated by the memory window divide by summarizing the writing and erasing voltage, is achieved. Such value is comparable to that of the high-performance polymer-blending-based transistor memories with a bilayer device configuration (evaporated semiconducting molecules/polymer hybrid), which possesses a charge storage density around 0.3–0.5 previously.[35,39] Compared to the copolymers containing F6NSt, in addition, no memory characteristics (i.e., threshold voltage shifting behavior on the transfer curve) was

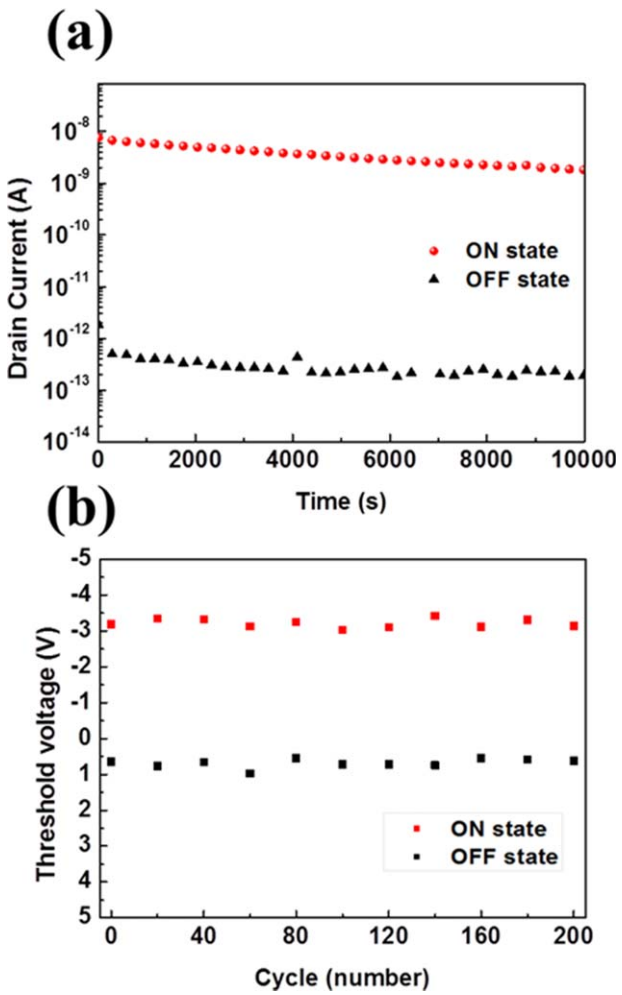

FIGURE 8 (a) Retention time and (b) endurance characteristics of the **P3**-based OFET memory devices. [Color figure can be viewed in the online issue, which is available at wileyonlinelibrary.com.]

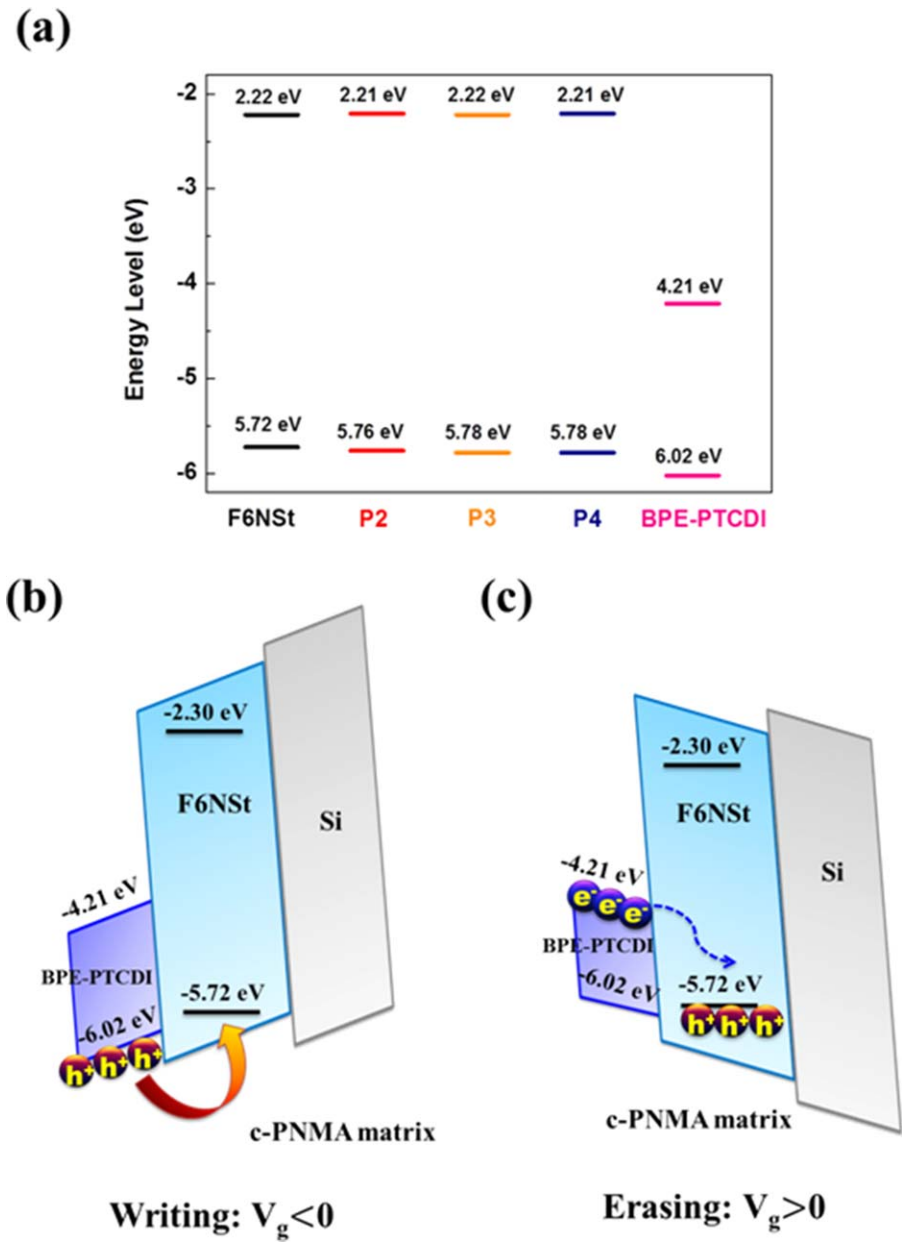

FIGURE 9 (a) Energy level diagram of BPE-PTCDI, F6NSt, and P(NMA-*co*-F6NSt)s (**P2**∼**P4**). Proposed memory mechanism and the energy band diagrams under (b) a negative gate voltage (i.e., writing process) and (c) a positive gate voltage (i.e., erasing process), respectively. [Color figure can be viewed in the online issue, which is available at wileyonlinelibrary.com.]

observed on the *c*-**P1** (pure PNMA)-based reference device [Fig. 7(b)], demonstrating that the stored charges are located in the F6NSt domain. Although *c*-**P4**-based device possesses the largest memory window among the studied copolymers, unstable electrical characteristics are explored at the same time (Supporting Information Fig. S12). The main reason is the lower content of crosslinkable NMA domain in **P4** may result in a higher leakage current and cannot serve as an effective blocking layer in the OFET memory, as proved by the MIM device detected dielectric property.

The long-term stability of the trapped charges, furthermore, is one of the most important factors for a nonvolatile OFET memory to exam its device performance. The retention time is defined as the time duration of the stored charges that retained in the charge storage layer, as explored in Figure 8(a) (*c*-**P3**-based device), Supporting Information Figures S11(b) and S12(b) (*c*-**P2** and **P4**-based device). Stable ON and OFF states at $V_g = 0$ V can be maintained for at least 10^4 s with the ON/OFF memory ratio above 10^4 for *c*-**P2** and **P3**-based OFET memory. The ON/OFF state switching endurance of such devices, moreover, was evaluated by write − read − erase − read (WRER) cycle measurement. The WRER cycles were electrically controlled as follows: the drain current was kept at $V_d = 5$ V, and the writing, reading, and erasing processes were implemented at $V_g = 5$, 0, and

−5 V, respectively. The *c*-**P3**-based device achieved stable operation stability as maintaining a threshold voltage of −3.2 V and 0.5 V for writing (ON) and erasing (OFF) stage under 200 endurance cycles, respectively [Fig. 8(b)]. The excellent charge storage ability of the memory is comparable to currently low voltage OFET memory devices based on organic nanofloating gate or polymer hybrid as the trapping layer.[13,36] The above results, therefore, suggesting that OFET memory devices using the *c*-(PNMA-*co*-F6NSt) random copolymers, especially **P3**, thin films as the both of blocking and trapping layer exhibit the excellent retention property and endurance characteristics due to the tightly network structure on the dielectrics as well as the good dispersion for the charge trapping cites (i.e., F6NSt).

The illustrated energy level diagram and proposed mechanism of P(NMA-*co*-F6NSt)-based memory device are depicted in Figure 9. The HOMO and LUMO energy levels of **P2**, **P3,** and **P4** that estimated from cyclic voltammogram show the similar values because of the energy levels are mainly dominated by conjugated fluorene building block (i.e., F6NSt). Note that the HOMO energy level of F6NSt is −5.72 eV. During the writing process, a large number of holes are induced at the HOMO level of the BPE-PTCDI layer by the negative electric field and trapped in the F6NSt domain in the studied *c*-(PNMA-*co*-F6NSt) layer, resulting in a negative V_{th} shift due to the extra holes accumulated in the channel between BPE-PTCDI and *c*-(PNMA-*co*-F6NSt) dielectrics before scanning. On the contrary, the trapped holes in F6NSt can be recombined under a positive voltage bias (i.e., erasing process), then the V_{th} is shifted back to its initial state.

CONCLUSIONS

High-*k* random copolymers of P(NMA-*co*-F6NSt)s were designed and synthesized for both dielectric and charge storage layer in low voltage-operated OFET memories. Such *c*-P(NMA-*co*-F6NSt) thin films possess low current leakage and good charge trapping properties owing to the chemical crosslinkable NMA segment and hole trapping element of F6NSt, respectively. In addition, the smooth crosslinked polymer thin films showed excellent resistance of organic solvents, providing the opportunity to modify hydrophobic self-assembly monolayer on the dielectric surface and further enhance the OFET performance. The studied memories, indeed, exhibited the advantages of a low voltage operation (smaller than 5 V), a small power consumption, and an efficient data storage capacity. A large memory window as high as 4.13 V with a stable data endurance could be obtained from **P3** (NMA/F6NSt molar ratio of 80:20) among the set of polymers, demonstrating the potential for next-generation high-performance electronic applications.

ACKNOWLEDGMENTS

The financial support from Ministry of Science and Technology of Taiwan is highly appreciated. The authors also acknowledge National Synchrotron Radiation Research Center of Taiwan for facilitating the X-ray experiments

REFERENCES AND NOTES

1 K. J. Baeg, Y. Y. Noh, H. Sirringhaus, D. Y. Kim, *Adv. Funct. Mater.* **2010**, *20*, 224–230.

2 S. T. Han, Y. Zhou, V. A. L, Roy, *Adv. Mater.* **2013**, *25*, 5425–5449.

3 W. P. Lin, S. J. Liu, T. Gong, Q. Zhao, W. Huang, *Adv. Mater.* **2014**, *26*, 570–606.

4 Q. D. Ling, D. J. Liaw, C. Zhu, D. S. H. Chan, E. T. Kang, K. G. Neoh, *Prog. Polym. Sci.* **2008**, *33*, 917–978.

5 P. Heremans, G. H. Gelinck, R. Müller, K. J. Baeg, D. Y. Kim, Y. Y. Noh, *Chem. Mater.* **2011**, *23*, 341–358.

6 A. J. Hong, E. B. Song, H. S. Yu, M. J. Allen, J. Kim, J. D. Fowler, J. K. Wassei, Y. Park, Y. Wang, J. Zou, R. B. Kaner, B. H. Weiller, K. L. Wang, *ACS Nano.* **2011**, *5*, 7812–7817.

7 B. Cho, S. Song, Y. Ji, T. W. Kim, T. Lee, *Adv. Funct. Mater.* **2011**, *21*, 2806–2829.

8 C. Di, F. Zhang, D. Zhu, *Adv. Mater.* **2013**, *25*, 313–330.

9 J. Zaumseil, H. Sirringhaus, *Chem. Rev.* **2007**, *107*, 1296–1323.

10 A. Khassanov, T. Schmaltz, H. G. Steinrück, A. Magerl, A. Hirsch, M. Halik, *Adv. Mater. Interface.* **2014**, *1*, 238–244.

11 Y. H. Chou, H. C. Chang, C. L. Liu, W. C. Chen, *Polym. Chem.* **2015**, *6*, 341–352.

12 H. C. Chang, C. Lu, C. L. Liu, W. C. Chen, *Adv. Mater.* **2015**, *27*, 27–33.

13 J. C. Hsu, W. Y. Lee, H. C. Wu, K. Sugiyama, A. Hirao, W. C. Chen, *J. Mater. Chem.* **2012**, *22*, 5820–5827.

14 Y. H. Chou, S. Takasugi, R. Goseki, T. Ishizone, W. C. Chen, *Polym. Chem.* **2014**, *5*, 1063–1071.

15 L. Dong, H. S. Sun, J. T. Wang, W. Y. Lee, W. C. Chen, *J. Polym. Sci. Part A Polym. Chem.* **2015**, *53*, 602–614.

16 H. Y. Chi, H. W. Hsu, S. H. Tung, C. L. Liu, *ACS Appl. Mater. Interfaces* **2015**, *7*, 5663–5673.

17 A. D. Yu, T. Kurosawa, M. Ueda, W. C. Chen, *J. Polym. Chem. Part A: Polym. Chem.* **2014**, *52*, 139–147.

18 W. L. Leong, P. S. Lee, A. Lohani, Y. M. Lam, T. Chen, S. Zhang, A. Dodabalapur, G. S. Mhaisalkar, *Adv. Mater.* **2008**, *20*, 2325–2331.

19 S. T. Han, Y. Zhou, Z. X. Xu, V. A. L. Roy, T. F. Hung, *J. Mater. Chem.* **2011**, *21*, 14575–14580.

20 M. Kang, K. J. Baeg, D. Khim, Y. Y. Noh, D. Y. Kim, *Adv. Funct. Mater.* **2013**, *23*, 3503–3512.

21 Y. C. Chiu, C. C. Shih, W. C. Chen, *J. Mater. Chem. C* **2015**, *3*, 551–558.

22 C. C. Shih, Y. C. Chiu, W. Y. Lee, J. Y. Chen, W. C. Chen, *Adv. Funct. Mater.* **2015**, *25*, 1511–1519.

23 Y. Zhou, S. T. Han, Z. X. Xu, V. A. L. Roy, *Nanoscale* **2013**, *5*, 1972–1979.

24 C. M. Chen, C. M. Liu, K. H. Wei, U. S. Jeng, C. H. Su, *J. Mater. Chem.* **2012**, *22*, 454–461.

25 Y. H. Chou, N. H. You, T. Kurosawa, W. Y. Lee, T. Higashihara, M. Ueda, W. C. Chen, *Macromolecules* **2012**, *45*, 6946–6956.

26 C. Wang, W. Y. Lee, R. Nakajima, J. Mei, D. H. Kim, Z. Bao, *Chem. Mater.* **2013**, *25*, 4806–4812.

27 M. E. Roberts, N. Queraltó, S. C. B. Mannsfeld, B. N. Reinecke, W. Knoll, Z. Bao, *Chem. Mater.* **2009**, *21*, 2292–2299.

28 C. Kim, Z. Wang, H. J. Choi, Y. G. Ha, A. Facchetti, T. J. Marks, *J. Am.Chem. Soc.* **2008**, *130*, 6867–6878.

29 M. H. Yoon, H. Yan, A. Facchetti, T. J. Marks, *J. Am. Chem. Soc.* **2005**, *127*, 10388–10395.

30 G. Tillet, B. Boutevin, B. Ameduri, *Prog. Polym. Sci.* **2011**, *36*, 191–217.

31 Y. C. Chiu, T. Y. Chen, Y. Chen, T. Satoh, T. Kakuchi, W. C. Chen, *ACS Appl. Mater. Interfaces* **2014**, *6*, 12780–12788.

32 Y. C. Chiu, C. L. Liu, W. Y. Lee, Y. Chen, T. Kakuchi, W. C. Chen, *NPG Asia Mater.* **2013**, *5*, e35.

33 C. Duan, L. Wang, K. Zhang, X. Guan, F. Huang, *Adv. Mater.* **2011**, *23*, 1665–1669.

34 S. Liu, K. Zhang, J. Lu, J. Zhang, H. L. Yip, F. Huang, Y. Cao, *J. Am. Chem. Soc.* **2013**, *135*, 15326–15329.

35 Y. H. Chou, Y. C. Chiu, W. C. Chen. *Chem. Commun.* **2014**, *50*, 3217–3219.

36 K. Sugiyama, A. Hirao, J. C. Hsu, Y. C. Tung, W. C. Chen, *Macromolecules* **2009**, *42*, 4053–4062.

37 C. Lu, H. C. Wu, Y. C. Chiu, W. Y. Lee, W. C. Chen, *Macromolecules* **2012**, *45*, 3047–3056.

38 M. M. Ling, P. Erk, M. Gomez, M. Koenemann, J. Locklin, Z. Bao, *Adv. Mater.* **2007**, *19*, 1123.

39 Y. H. Chou, C. L. Tsai, W. C. Chen, G. S. Liou, *Polym. Chem.* **2014**, *5*, 6718–6727.